



Encoding the complete electric field of an ultraviolet ultrashort laser pulse in a near-infrared nonlinear-optical signal

TRAVIS JONES,^{1,2,5}  WILLIAM K. PETERS,¹ ANATOLY EFIMOV,³ 
RICHARD L. SANDBERG,⁴  DMITRY YAROTSKI,³ RICK TREBINO,²
AND PAMELA BOWLAN^{1,6}

¹*Physical Chemistry and Applied Spectroscopy, Los Alamos National Lab, Los Alamos, New Mexico 87544, USA*

²*School of Physics, Georgia Institute of Technology, Atlanta, Georgia 30332, USA*

³*Center for Integrated Nanotechnologies, Los Alamos National Lab, Los Alamos, New Mexico 87544, USA*

⁴*Department of Physics and Astronomy, Brigham Young University, Provo, Utah 84602, USA*

⁵*jonetn11@lanl.gov*

⁶*pambowlan@lanl.gov*

Abstract: We introduce a variation on the cross-correlation frequency-resolved optical gating (XFROG) technique that uses a near-infrared (NIR) nonlinear-optical signal to characterize pulses in the ultraviolet (UV). Using a transient-grating XFROG beam geometry, we create a grating using two copies of the unknown UV pulse and diffract a NIR reference pulse from it. We show that, by varying the delay between the UV pulses creating the grating, the UV pulse intensity-and-phase information can be encoded into a NIR signal. We also implemented a modified generalized-projections phase-retrieval algorithm for retrieving the UV pulses from these spectrograms. We performed proof-of-principle measurements of chirped pulses and double pulses, all at 400 nm. This approach should be extendable deeper into the UV and potentially even into the extreme UV or x-ray range.

© 2020 Optical Society of America under the terms of the [OSA Open Access Publishing Agreement](#)

1. Introduction

Ultrashort laser pulses in the ultraviolet (UV) spectral range provide access to higher-energy electronic transitions and achieve a tighter focus than visible or near-infrared (NIR) pulses and so play important roles in time-resolved spectroscopy [1–4], nanolithography [5] and micromachining [6,7]. Of course, any application of UV ultrashort pulses requires measuring their complete electric field for optimizing and confirming the characteristics of the light source. UV pulse measurement can also serve as a phase and amplitude sensitive detector for measuring the complex response of a sample, as in multidimensional spectroscopies [8,9].

A common approach for characterizing ultrashort laser pulses, which are much too short to measure with electronics, is to use a nonlinear-optical interaction as a femtosecond (fs)-timescale gate, as is done in Frequency-Resolved Optical Gating (FROG) [10]. In FROG, the pulse interacts with (“gates”) itself in a nonlinear-optical medium, producing a nonlinear-optical signal, which represents a time slice of the unknown pulse’s electric field, $E_{unk}(t)$. Another (“reference”) laser pulse may also gate the unknown pulse, in which case the method is called cross-correlation FROG, or XFROG. For simplicity, we will henceforth include the techniques, FROG and XFROG, in the single term FROG unless we wish to make a distinction between them. Measuring the spectrally resolved nonlinear-optical signal as a function of the delay between the two (or three) interacting pulses in these arrangements yields a spectrogram, or FROG trace. The pulse’s temporal (or equivalently spectral) electric field can be uniquely determined from the FROG trace using well-established phase-retrieval algorithms, such as the generalized projections (GP)

algorithm. The FROG concept has been widely applied to measure ultrashort laser pulses ranging in center frequency from the infrared to the extreme ultraviolet [10].

One of the main challenges in measuring UV pulses is detection, since wavelengths below about 200 nm are outside of the range of standard silicon detectors and so require more expensive, specialized UV cameras. It can also be challenging to find a nonlinear medium that is transparent in the UV and has the required nonlinear-optical phase-matching characteristics. Deeper in the UV, optical components such as lenses and mirrors also become less available. FROG has been applied to measure 400 nm femtosecond pulses by difference frequency generation with an 800 nm pulse, which conveniently produces a nonlinear signal in the NIR [11]. However, finding an appropriate medium that is transparent and has the birefringence required for phase matching at wavelengths shorter than 400 nm in a second-order nonlinear optical process is challenging. Therefore, measurement of UV pulses most commonly uses third-order nonlinear optical signals such as polarization-gating (PG) [12,13], self-diffraction (SD) [14–18], and transient-grating (TG) [19–23], which can often be accomplished in any transparent medium. Still, most of these methods require detecting a nonlinear signal at the UV pulse wavelength. FROG spectrograms can be measured for deeper UV pulses which are absorbed by or ionize the nonlinear medium using methods based on spectrally resolved photoemission [24,25] or reflection by plasma mirrors produced by intense NIR pulses [26].

Our objective is to develop an all-optical FROG method for measuring UV pulses, where the UV pulse shape is encoded not in a UV nonlinear-optical signal, as in the above methods, but in an easily detectable NIR nonlinear-optical signal. We also aim to develop a method that is well-suited for extension to higher frequencies in the extreme ultraviolet (XUV) and x-ray spectral ranges for which there is a strong need for single-shot complete field characterization, in particular at Free Electron Lasers (FEL) [27].

In this publication, we demonstrate a variation of TG XFROG in which the transient grating is induced by two copies of the unknown UV pulse. This grating is then probed by a known NIR reference pulse, yielding a signal pulse at the same wavelength as the probe pulse, which can then be easily detected. Importantly, our technique involves scanning the delay *between the UV pulses*, rather than the reference-pulse delay as in standard TG FROG [19,20,23]. This allows us to retrieve the UV-pulse phase information, which would otherwise not be available. We refer to this variation on TG XFROG as Induced-Grating XFROG. Here we present a proof-of-principle demonstration by measuring pulses centered at 400 nm with an 800 nm reference pulse. We show that these spectrograms contain the 400 nm pulse phase information and apply the generalized projections algorithm to reconstruct the 400 nm pulse's intensity and phase. Although our proof-of-principle tests were performed on 400 nm pulses, this method should be applicable to deeper UV and potentially even XUV and x-ray ultrashort pulses, since the nonlinear medium does not have to be transparent at the unknown-pulse wavelength and the phase matching is scalable. Also, while we used a multi-shot geometry here, standard single-shot FROG geometries should also be applicable (see for example [21]). Thus the approach introduced here has the potential to extend the suite of FROG-based techniques for single-shot, full-field characterization to high photon energies [10,28].

2. Encoding a UV pulse shape in a NIR nonlinear optical signal

Our technique is based on standard TG FROG [20,23]. Compared to the other third-order FROG geometries, TG FROG has several advantages for UV pulse measurement: it uses a nonlinear process that can be phase-matched by satisfying the Bragg condition, $\sin\theta_{probe} = (\lambda_{probe} / \lambda_{excite}) \sin\theta_{excite}$; its signal is spatially separated from the input beams and so is background-free; and polarizers, which introduce dispersion, are not needed.

In a typical TG FROG measurement, the pulse to be characterized is split into three parallel beams that cross and spatially overlap at the focus of a lens at the nonlinear medium [20,23].

Two of the beams temporally overlap and interfere, inducing the transient grating, while the third beam diffracts from it forming the nonlinear signal. A TG FROG trace is the spectrum of the diffracted pulse versus the delay between the diffracted pulse and the transient grating. In TG cross-correlation FROG, or TG XFROG, a characterized reference pulse is available, and it induces the grating and the diffracted unknown pulse forms the nonlinear signal [16,17]. In standard TG XFROG, the spectrogram contains phase information only of the pulse that *diffracts* from the grating, and not of the pulses that *induce* it. As a result, when measuring a UV pulse, the UV pulse must probe the grating, not induce it, and the nonlinear signal will necessarily be at the same UV wavelength, thus requiring UV detection.

Induced-Grating XFROG uses a similar $\chi^{(3)}$ process, but instead produces a nonlinear signal at the reference pulse wavelength, in the visible or NIR, avoiding the need for UV light detection. Instead of diffracting the unknown pulse from the transient grating, two copies of the unknown UV pulse induce the transient grating, as shown in Fig. 1. Then the longer-wavelength reference pulse diffracts from the grating to form an easily detectable nonlinear signal centered at the reference pulse wavelength. The key to measuring a spectrogram that contains the UV pulse's phase information is to vary the delay between the UV pulse replicas, maintaining the reference probe pulse at zero delay. Intuitively, one can consider that the UV pulse-pair only induce a grating when they temporally overlap, so the contrast or grating fringe depth is best at zero delay and the instantaneous wavelength of the UV pulse determines the periodicity of the grating. Thus, the transient grating contrast and phase versus delay between the UV pulses contains both the intensity and phase information about the UV pulse, which is probed and read-out by the longer-wavelength, diffracted reference pulse. More precisely, each UV pulse generates a coherence in the nonlinear-optical medium that lives for the dephasing time, usually referred to as T_2 . But this time is generally very short for condensed phases and in this work we consider the coherent response to be instantaneous and representable by a delta function.

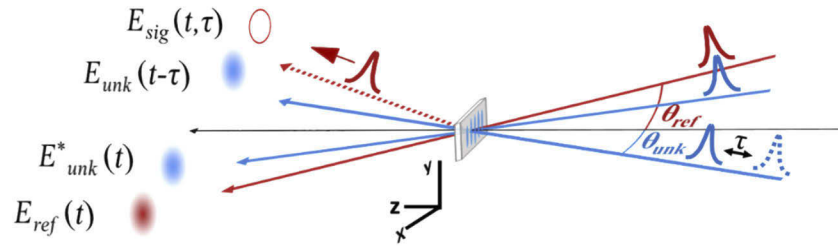


Fig. 1. Schematic of the beam geometry used in Induced-Grating XFROG. Beam arrangement before and after the sample, showing that the grating pulse-pair delay is varied. The unknown, reference, and signal beams are E_{unk} , E_{ref} , and E_{sig} respectively. Phase matching is achieved by satisfying the Bragg condition: $\sin \theta_{ref} = (\lambda_{ref} / \lambda_{unk}) \sin \theta_{unk}$, where E_{ref} is the probe pulse and E_{unk} is the excite pulse. θ_{ref} and θ_{unk} represent the half-crossing angles for the reference and unknown pulses.

3. Generalized-projections phase-retrieval algorithm for Induced-Grating XFROG

The Induced-Grating XFROG discussed above results in the following nonlinear signal:

$$E_{sig}(t, \tau) = E_{ref}(t)E_{unk}^*(t)E_{unk}(t - \tau). \quad (1)$$

The reference, unknown, and signal fields are E_{ref} , E_{unk} , and E_{sig} , respectively, with the delay, τ in one of the unknown fields. Measuring the spectrum of this nonlinear signal versus τ results in

a FROG trace, $I_{sig}(\omega, \tau)$, given by,

$$I_{sig}(\omega, \tau) = \left| \int_{-\infty}^{\infty} E_{ref}(t) E_{unk}^*(t) E_{unk}(t - \tau) \exp(-i\omega t) dt \right|^2. \quad (2)$$

Using Eqs. (1)–(2), the generalized-projections phase-retrieval algorithm can be applied to extract $E_{unk}(t)$ from the FROG trace [10]. Following the usual procedure, the first step is to make an initial guess for $E_{unk}(t)$, which is usually taken to be random noise. This guess and the known reference field $E_{ref}(t)$ are then used to calculate $E_{sig}(t, \tau)$ from Eq. (1). Next, $E_{sig}(t, \tau)$ is Fourier transformed to the frequency domain and its magnitude is replaced by the square root of the measured trace yielding $\tilde{E}'_{sig}(\omega, \tau)$. $\tilde{E}'_{sig}(\omega, \tau)$ is then inverse Fourier transformed to the (t, τ) domain where it is used to update the next guess for the unknown pulse. In order to obtain $E_{unk}(t)$ for the next iteration, we minimize the following functional distance:

$$Z^{(k)} = \sum_{i,j=1}^N |E_{sig}^{(k)}(t_i, \tau_j) - E_{ref}(t_i) E_{unk}^{*(k+1)}(t_i) E_{unk}^{(k+1)}(t_i - \tau_j)|^2, \quad (3)$$

where superscripts k and $k + 1$ denote the current and next iteration respectively. Eq. (3) takes into account the functional form of the nonlinear signal field, $E_{sig}(t, \tau)$, for the Induced-Grating XFROG trace, and is otherwise known as the mathematical form constraint. Again, following the approach discussed in [10], to find an updated guess for the unknown field, Eq. (3) is minimized with respect to the unknown field via the method of steepest descent in which the equation for updating the field is given by Eq. (4) where $x^{(k)}$ is a scalar multiplier. The expressions for derivatives are given by Eq. (5) and Eq. (6) where the k and $k + 1$ superscripts have been suppressed for simplicity,

$$E_{unk}^{(k+1)} = E_{unk}^{(k)} - x^{(k)} \nabla Z^{(k)} \quad (4)$$

$$\frac{\partial Z}{\partial \text{Re}\{E_{unk}(t_k)\}} = \sum_{j=1}^N \begin{bmatrix} -E_{sig}(t_k, \tau_j) E_{ref}^*(t_k) E_{unk}^*(t_k - \tau_j) \\ + E_{unk}(t_k) |E_{ref}(t_k) E_{unk}(t_k - \tau_j)|^2 \\ -E_{sig}(t_k + \tau_j, \tau_j) E_{ref}^*(t_k + \tau_j) E_{unk}^*(t_k + \tau_j) \\ + E_{unk}(t_k) |E_{ref}(t_k + \tau_j) E_{unk}(t_k + \tau_j)|^2 \\ + c.c \end{bmatrix} \quad (5)$$

$$\frac{\partial Z}{\partial \text{Im}\{E_{unk}(t_k)\}} = \sum_{j=1}^N \begin{bmatrix} -i E_{sig}(t_k, \tau_j) E_{ref}^*(t_k) E_{unk}^*(t_k - \tau_j) \\ -i E_{unk}(t_k) |E_{ref}(t_k) E_{unk}(t_k - \tau_j)|^2 \\ + i E_{sig}(t_k + \tau_j, \tau_j) E_{ref}^*(t_k + \tau_j) E_{unk}^*(t_k + \tau_j) \\ -i E_{unk}(t_k) |E_{ref}(t_k + \tau_j) E_{unk}(t_k + \tau_j)|^2 \\ + c.c \end{bmatrix}. \quad (6)$$

Note, that in writing these equations, it is necessary to know which of the two unknown pulses is delayed, due to the complex conjugate in Eq. (1). Placing the delay in the other copy of the unknown pulse slightly changes the equations above.

4. Experimental setup

Figure 2 shows a schematic of the experimental setup used for proof-of-principle demonstrations of the Induced-Grating XFROG method discussed above. For the light source, we used a regenerative Ti:Sapphire amplifier with pulses centered near 800 nm at a 1 KHz repetition rate.

The laser beam was first split (BS1 in Fig. 2) into two replicas. A less intense replica (~10%) of the pulse energy was used for the reference pulse, which was characterized with a commercial GRENOUILLE device [29] by introducing a flip mirror (FM). The reference pulse used in the measurements provided in the next section was approximately 160 fs long with a small amount of predominantly quadratic spectral phase (chirp). The temporal intensity and phase of this pulse is shown in the inset in Fig. 2.

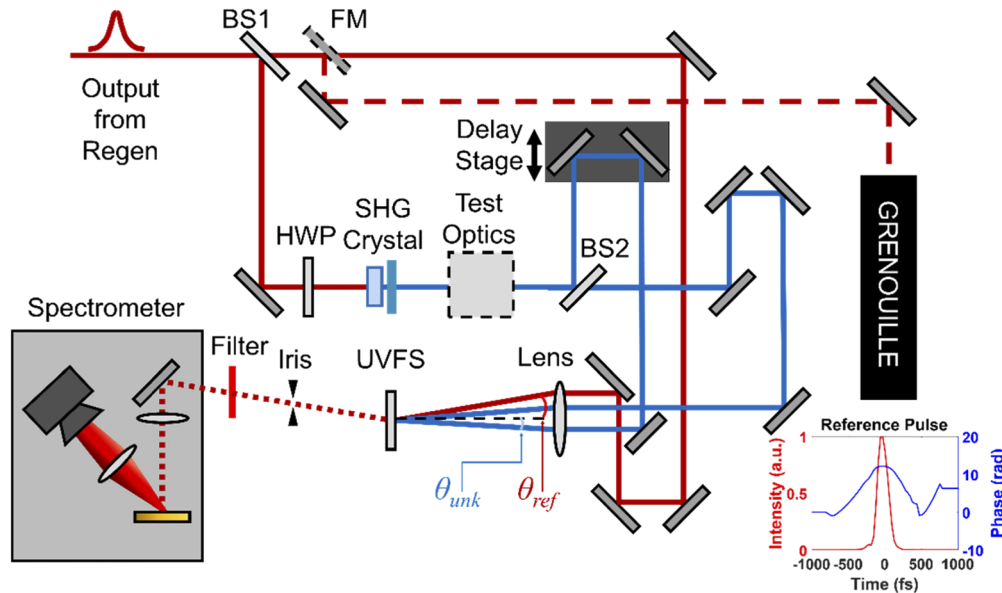


Fig. 2. Experimental setup for Induced-Grating XFROG. A half-wave plate (HWP) is used before the SHG crystal so that the generated second harmonic light has the same polarization as the reference pulse. After the SHG crystal, the 400 nm pulses are sent through two sets of test optics. In the first measurement, the 400 nm pulse was intentionally chirped using 0 mm, 20 mm, and 50 mm pieces of SF11 glass. In the second measurement, a small Michelson interferometer was used to make variably separated double pulses. In both experiments the nonlinear medium was UV-grade fused silica (UVFS). The half crossing angles for the unknown and reference pulses are also labeled accordingly. The inset at the bottom right of the figure shows the intensity and phase of the reference pulse measured using GRENOUILLE.

To generate the unknown UV pulses, the more intense replica of the beam (~90%) was converted to 400 nm in a 0.5 mm-thick BBO SHG crystal. A half-wave plate (HWP) is used before the second harmonic generation (SHG) crystal so that the resulting 400 nm pulses have the same polarization as the reference pulse. To produce the transient grating, a 50/50 beam splitter (BS2) was used to generate two replicas of the 400 nm pulse. All three beams propagated parallel and along a horizontal line to a 250 mm focal length lens, so that they spatially overlapped and focused at the sample. The spot size of the 400 nm beams at the focus was approximately 40 μm FWHM. Phase matching in these experiments simply requires satisfying the Bragg condition for the input beams, or that $\sin \theta_{ref} = (\lambda_{ref} / \lambda_{unk}) \sin \theta_{unk}$. To satisfy this, we used half-crossing-angles of approximately 1.72° and 3.43° for the unknown (excite) and reference (probe) beams, respectively. The nonlinear medium was UV fused silica. The 800 nm nonlinear signal was detected with a homemade imaging spectrometer. To collect the FROG traces, a motorized delay stage was used to vary the delay of one 400 nm pulse, and the spectrum of the diffracted NIR reference pulse was measured as a function of delay.

5. Results

We performed two sets of measurements to test the performance of Induced-Grating XFROG. In the first one, we intentionally chirped the 400 nm pulse by a known amount using 0 mm, 20 mm, and 50 mm pieces of SF11 glass (the “test optic” in Fig. 2). The top row in Fig. 3 shows the results of these measurements. To extract $E_{unk}(t)$ from the measured traces, we applied the GP algorithm discussed in section 3.

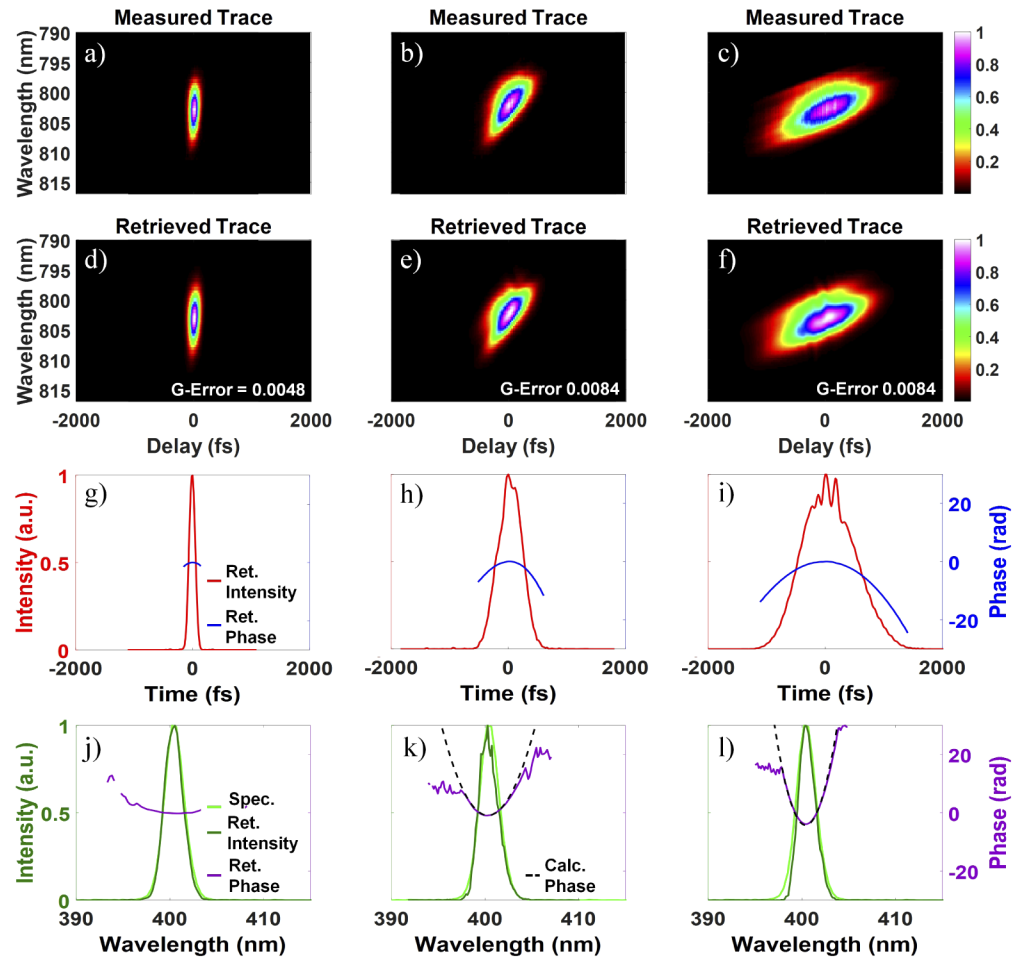


Fig. 3. Measurements of chirped 400 nm pulses using an 800 nm reference pulse. The columns correspond to dispersion introduced with 0 mm (left), 20 mm (center), and 50 mm (right) of SF11. (a-c) Measured Traces. Measured traces (a) and (b) were binned to 128×128 arrays and (c) was binned to a 256×256 array. (d-f) Retrieved Traces. (g-i) Temporal intensity (red) and phase (blue) of the retrieved pulse. (j-l) Independently measured spectra (light green), retrieved spectra (dark green), retrieved spectral phase (purple), expected spectral phase calculated from the Sellmeier equations for the glass used to introduce dispersion (dashed black line). The G errors for each case are included in the bottom right hand corner of each retrieved trace.

The accuracy of the reconstruction is typically quantified by the G error. As usual, the G error on each iteration is defined as [10]:

$$G^{(k)} = \sqrt{\frac{1}{N^2} \sum_{i,j=1}^N |I_{FROG}(\omega_i, \tau_j) - \mu I_{FROG}^{(k)}(\omega_i, \tau_j)|^2} \quad (7)$$

where the index k indicates the k^{th} iteration and μ is a real normalization constant used to minimize $G^{(k)}$. And G (without a superscript) is the resulting rms error when the algorithm is finished running. G errors of about 1% or less indicate convergence and a good measurement for the types of pulses and traces considered here.

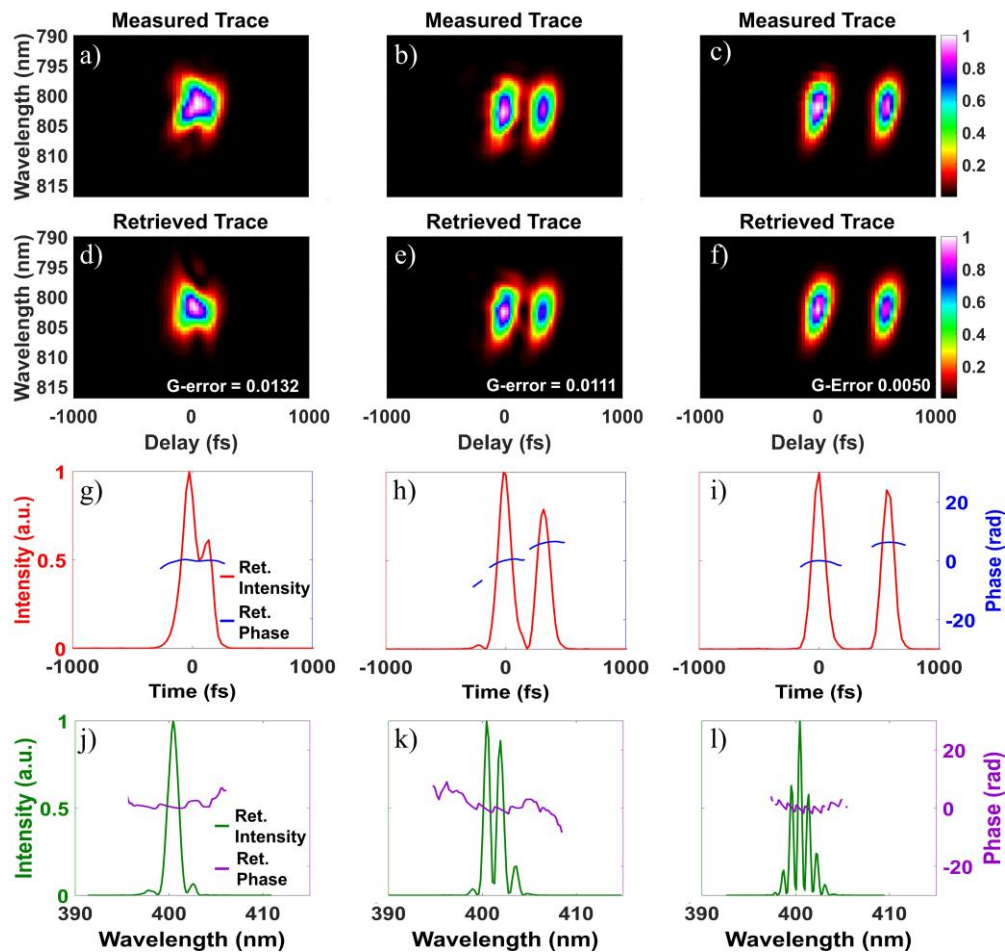


Fig. 4. Experimental results from the series of variable-separation double pulse measurements. Columns correspond to near-zero separation (left), ~300 fs separation (center), and ~600 fs (right). (a-c) Measured Traces. Each of the measured traces were binned to 128×128 arrays. (d-f) Retrieved Traces. (g-i) Temporal intensity (red) and phase (blue) of the retrieved pulse. (j-l) Retrieved spectral intensity (dark green), retrieved spectral phase (purple). The G errors for each case are included in the bottom right hand corner of each retrieved trace.

The reconstructed traces along with their G errors (rms differences between the measured and retrieved traces) are provided in Figs. 3(d)–3(f). The reconstructed pulse shapes in the time and frequency domains are shown in Figs. 3(g)–3(i) and Figs. 3(j)–3(l) respectively. Independently measured spectra (light green) are overlaid for comparison, as well as the calculated spectral phases (black, dashed lines).

As a second test of this method, double pulses, produced by a Michelson interferometer (the “test optic” in Fig. 2), were measured. These measurements are shown in Fig. 4 for three different double pulse separations, again showing the measured traces, the reconstructed traces from the GP algorithm, G errors, and the reconstructed pulses in the time and frequency domains.

6. Discussion

The measurements in Figs. 3–4 demonstrate that Induced-Grating XFROG spectrograms contain the 400 nm pulse phase and amplitude information. A convenient feature of these spectrograms, similar to other types of FROG based on third-order nonlinear optical effects [10], is that the pulse shape can often be intuitively read directly from the FROG trace. Figure 3 shows that chirp in the 400 nm pulse results in a tilted FROG trace where the amount of tilt depends on the amount of chirp. Similarly, the FROG traces for the double pulses in Fig. 4 have an intensity profile vs. delay that follows that of the double pulses’ temporal intensity. As is the case with other third-order FROG variations, these traces also indicate the absence of a direction-of-time ambiguity. Note that the appearance of the traces depends on the pulse duration of the NIR reference pulse relative to the 400 nm pulses. Figure 4 is an example of this. Here, the NIR and 400 nm pulses (before the “test optic”) have similar pulse durations. Thus, as we varied the double pulse separation, the reference pulse was only long enough in time to maintain sufficient temporal overlap with one of the pulses in the double pulse. If the reference pulse were instead long enough to maintain temporal overlap with both pulses in the double pulse, then the Induced-Grating XFROG trace would look more similar to a typical self-referenced double-pulse FROG trace [10], with a three-lobed structure.

Prior to their retrieval, each of the measured traces in Figs. 3–4 were binned to 128×128 arrays except for the trace in Fig. 3(c) which was binned to a 256×256 array. The second row of Figs. 3–4 shows the results of the GP phase retrieval algorithm. The G error for each retrieval is provided at the bottom right of each retrieved trace. Convergence was typically achieved within a few minutes. In the second set of measurements, we suspect that instabilities in the Michelson interferometer used to generate the double pulse may be responsible for a higher G error, particularly in the trace with the smallest double pulse separation. Still, these measurements demonstrate that this method works for measuring more complex pulse shapes with larger time-bandwidth products.

The chirped pulses allow for another test of the measurements and reconstruction. Figures 3(j)–3(l) show the retrieved spectra compared with independently measured spectra using an Ocean Optics spectrometer. The spectra are in good agreement. Furthermore, since the shape of the spectral phase in the 400 nm pulses in Fig. 3 comes primarily from the dispersive glass that we introduced, we can also compare the retrieved spectral phases with that calculated from the Sellmeier equations for SF11 [30]. The expected GDD from the 20 mm and 50 mm pieces of SF11 was calculated to be 17721.3 fs^2 and 44257.0 fs^2 , respectively. These values correspond to second-order spectral phase coefficients of 8860.7 fs^2 and 22128.5 fs^2 . Curves corresponding to these values are shown as black dashed lines in Figs. 3(j)–3(l) and are in good agreement with the measured spectral phases. Together these checks on the spectra and spectral phase prove that the correct spectral (or equivalently temporal) electric fields were retrieved.

Measurements like those of the approximately 125 fs pulse in the first column of Fig. 3 were obtained with a total 400 nm pulse energy of approximately 140 nJ and a 20 ms integration time on the camera. Combined with the $40 \mu\text{m}$ spot size mentioned above, this results in a fluence of $\sim 10 \text{ mJ/cm}^2$ at the sample. In addition to the integration time on the camera, the required

amount of UV pulse fluence also depends on the reference pulse energy. Thus, by reducing the UV pulse energy and compensating this reduction with an increase in the reference pulse energy and/or camera integration time, UV pulses with considerably less pulse energy should be measurable. In this case, one should also take care not to increase the reference pulse energy too much as this could lead to increased scattered light at the signal wavelength. Furthermore, since the input polarization used is not restricted by the nonlinear interaction involved, this technique should also be applicable in instances where the measured pulse varies differently along different polarization components.

Previous work using TG XFROG has shown that the phase-matching bandwidth of a transient grating process can be very broadband [21]. We estimate the phase-matching bandwidth in our experiments to be greater than 100 nm. This could be increased, if necessary, by choosing different focusing conditions. However, even if the phase-matching bandwidth becomes limiting, for example if measuring single-cycle UV pulses, FROG spectrograms can be corrected for insufficient phase-matching bandwidth [31]. Thus, to our knowledge, there is no strict lower limit on the duration of the unknown pulse that can be measured with Induced-Grating XFROG. However, when attempting to measure extremely short pulses other challenges arise. These are the detection of the very broadband nonlinear signal, accounting for material dispersion in the nonlinear medium and other optical components [32], geometrical smearing (for multi-shot measurements), and the breakdown of the slowly-varying envelope approximation, all of which are typically solvable problems [10].

Additionally, we foresee no strict requirements on the duration or complexity of the reference pulse required for Induced-Grating XFROG, provided that its intensity and phase are well characterized. Shorter or longer reference pulses can in principle be used. However, to avoid unnecessarily complicating the measurement, we recommend choosing the simplest available reference pulse at the desired center wavelength (typically the NIR pulse directly out of the laser system makes a good reference pulse). Also, as in standard XFROG, for simultaneously achieving good spectral and temporal resolutions it is best to aim for equally distributing information in the measured trace between both domains of the trace (time and frequency) [10].

7. Conclusions

We demonstrated Induced-Grating XFROG for encoding the intensity and phase of a 400 nm pulse in a NIR nonlinear-optical signal. We applied the GP phase retrieval algorithm to reconstruct the pulse's electric field from the measured spectrogram. To test this method, we demonstrated accurate measurement of chirped 400 nm pulses and also the measurement of more complex double pulses. While the proof-of-principle tests done here were at 400 nm, this approach should be extendable deeper into the UV and potentially even into the extreme UV [33] or x-ray range, since phase matching only requires satisfying the Bragg condition. Another advantage of detecting the nonlinear signal at the reference pulse wavelength is that the medium does not necessarily have to be transparent at the unknown pulse wavelength as long as the functional form of nonlinear signal is still known. Single-shot implementation of Induced-Grating XFROG should also be straightforward following the approach used for other single-shot FROG implementations [10]. In conclusion, we believe that Induced-Grating XFROG represents a first step towards developing an all-optical FROG method for measuring UV and possibly even higher-photon-energy femtosecond laser pulses.

Funding

Los Alamos National Laboratory's Laboratory Directed Research and Development Program (20180242ER); Los Alamos National Laboratory's African-American Partnership Program; National Science Foundation (ECCS-1609808); Georgia Research Alliance.

Acknowledgments

This work was performed, in part, at the Center for Integrated Nanotechnologies, an Office of Science User Facility operated for the U.S. Department of Energy (DOE) Office of Science. The Los Alamos National Laboratory, an affirmative action equal opportunity employer, is managed by Triad National Security, LLC for the U.S. Department of Energy's NNSA, under Contract No. 89233218CNA000001.

Disclosures

Rick Trebino owns a company that sells pulse-measurement devices.

References

1. M. Bauer, "Femtosecond ultraviolet photoelectron spectroscopy of ultra-fast surface processes," *J. Phys. D: Appl. Phys.* **38**(16), R253–R267 (2005).
2. M. Chergui, "Ultrafast molecular photophysics in the deep-ultraviolet," *J. Chem. Phys.* **150**(7), 070901 (2019).
3. H. Ihee, J. Cao, and A. H. Zewail, "Ultrafast Electron Diffraction of Transient $[\text{Fe}(\text{CO})_4]$: Determination of Molecular Structure and Reaction Pathway," *Angew. Chem., Int. Ed.* **40**(8), 1532–1536 (2001).
4. P. Siffalovic, M. Drescher, M. Spieweck, T. Wiesenthal, Y. C. Lim, R. Weidner, A. Elizarov, and U. Heinzmann, "Laser-based apparatus for extended ultraviolet femtosecond time-resolved photoemission spectroscopy," *Rev. Sci. Instrum.* **72**(1), 30–35 (2001).
5. J. E. Balmer, D. Bleiner, and F. Staub, "Extreme ultraviolet lasers: principles and potential for next-generation lithography," *J. Micro/Nanolithography, MEMS, and MOEMS* **11**(2), 021119 (2012).
6. G. Mincuzzi, A. Bourtereau, A. Rebière, H. Laborie, M. Faucon, M. Delaigue, K. Mishchik, C. Homogenizer, E. Audouard, and R. Kling, "Pulse to pulse control in micromachining with femtosecond lasers," *Proc. SPIE 11268, Laser-based Micro- and Nanoprocessing XIV* 112681F(2020).
7. J. H. Klein-Wiele, J. Bekesi, and P. Simon, "Sub-micron patterning of solid materials with ultraviolet femtosecond pulses," *Appl. Phys. A* **79**(4-6), 775–778 (2004).
8. U. Selig, C.-F. Schleussner, M. Foerster, F. Langhojer, P. Nuernberger, and T. Brixner, "Coherent two-dimensional ultraviolet spectroscopy in fully noncollinear geometry," *Opt. Lett.* **35**(24), 4178–4180 (2010).
9. B. A. West and A. M. Moran, "Two-Dimensional Electronic Spectroscopy in the Ultraviolet Wavelength Range," *J. Phys. Chem. Lett.* **3**(18), 2575–2581 (2012).
10. R. Trebino, *Frequency-resolved optical gating: the measurement of ultrashort laser pulses* (Springer Science & Business Media, 2000).
11. S. Linden, J. Kuhl, and H. Giessen, "Amplitude and phase characterization of weak blue ultrashort pulses by downconversion," *Opt. Lett.* **24**(8), 569–571 (1999).
12. D. J. Kane, A. J. Taylor, R. Trebino, and K. W. DeLong, "Single-shot measurement of the intensity and phase of a femtosecond UV laser pulse with frequency-resolved optical gating," *Opt. Lett.* **19**(14), 1061–1063 (1994).
13. K. Michelmann, T. Feuer, R. Fernsler, and R. Sauerbrey, "Frequency resolved optical gating in the UV using the electronic Kerr effect," *Appl. Phys. B: Lasers Opt.* **63**(5), 485–489 (1996).
14. S. Backus, J. Peatross, Z. Zeek, A. Rundquist, G. Taft, M. M. Murnane, and H. C. Kapteyn, "16-fs, 1- μJ ultraviolet pulses generated by third-harmonic conversion in air," *Opt. Lett.* **21**(9), 665–667 (1996).
15. T. S. Clement, A. J. Taylor, and D. J. Kane, "Single-shot measurement of the amplitude and phase of ultrashort laser pulses in the violet," *Opt. Lett.* **20**(1), 70–72 (1995).
16. O. Dühr, E. T. J. Nibbering, G. Korn, G. Tempea, and F. Krausz, "Generation of intense 8-fs pulses at 400 nm," *Opt. Lett.* **24**(1), 34–36 (1999).
17. C. G. Durfee, S. Backus, H. C. Kapteyn, and M. M. Murnane, "Intense 8-fs pulse generation in the deep ultraviolet," *Opt. Lett.* **24**(10), 697–699 (1999).
18. J. Liu, K. Okamura, Y. Kida, T. Teramoto, and T. Kobayashi, "Clean sub-8-fs pulses at 400 nm generated by a hollow fiber compressor for ultraviolet ultrafast pump-probe spectroscopy," *Opt. Express* **18**(20), 20645–20650 (2010).
19. A. Ermolov, H. Valtma-Lukner, J. Travers, and P. St.J. Russell, "Characterization of few-fs deep-UV dispersive waves by ultra-broadband transient-grating XFROG," *Opt. Lett.* **41**(23), 5535–5538 (2016).
20. D. Lee, S. Akturk, P. Gabolde, and R. Trebino, "Experimentally simple, extremely broadband transient-grating frequency-resolved-optical-gating arrangement," *Opt. Express* **15**(2), 760–766 (2007).
21. D. Lee, P. Gabolde, and R. Trebino, "Toward single-shot measurement of a broadband ultrafast continuum," *J. Opt. Soc. Am. B* **25**(6), A34–A40 (2008).
22. T. Nagy and P. Simon, "Single-shot TG FROG for the characterization of ultrashort DUV pulses," *Opt. Express* **17**(10), 8144–8151 (2009).
23. J. N. Sweetser, D. N. Fittinghoff, and R. Trebino, "Transient-grating frequency-resolved optical gating," *Opt. Lett.* **22**(8), 519–521 (1997).
24. Y. Mairesse and F. Quéré, "Frequency-resolved optical gating for complete reconstruction of attosecond bursts," *Phys. Rev. A* **71**(1), 011401(R) (2005).

25. M. Isinger, D. Busto, S. Mikaelsson, S. Zhong, C. Guo, P. Salières, C. L. Arnold, A. L'Huillier, and M. Gisselbrecht, "Accuracy and precision of the RABBIT technique," *Philos. Trans. R. Soc., A* **377**(2145), 20170475 (2019).
26. R. Itakura, T. Kumada, M. Nakano, and H. Akagi, "Frequency-resolved optical gating for characterization of VUV pulses using ultrafast plasma mirror switching," *Opt. Express* **23**(9), 10914–10924 (2015).
27. C. Bostedt, S. Boutet, D. M. Fritz, Z. Huang, H. J. Lee, H. T. Lemke, A. Robert, W. F. Schlotter, J. J. Turner, and G. J. Williams, "Linac Coherent Light Source: The first five years," *Rev. Mod. Phys.* **88**(1), 015007 (2016).
28. R. Trebino, P. Bowlan, P. Gabolde, X. Gu, S. Akturk, and M. Kimmel, "Simple devices for measuring complex ultrashort pulses," *Laser Photonics Rev.* **3**(3), 314–342 (2009).
29. P. O'Shea, M. Kimmel, X. Gu, and R. Trebino, "Highly simplified device for ultrashort-pulse measurement," *Opt. Lett.* **26**(12), 932–934 (2001).
30. RefractiveIndex.Info: Refractive Index Database, "Optical constants of SF11" <https://refractiveindex.info/?shelf=glass&book=SF11&page=SCHOTT>. Accessed April 1, 2020.
31. A. Baltuska, M. S. Pshenichnikov, and D. A. Wiersma, "Second-harmonic generation frequency-resolved optical gating in the single-cycle regime," *IEEE J. Quantum Electron.* **35**(4), 459–478 (1999).
32. M. Li, J. P. Nibarger, C. Guo, and G. N. Gibson, "Dispersion-free transient-grating frequency-resolved optical gating," *Appl. Opt.* **38**(24), 5250–5253 (1999).
33. F. Capotondi, L. Foglia, M. Kiskinova, C. Masciovecchio, R. Mincigrucci, D. Naumenko, E. Pedersoli, A. Simoncig, and F. Bencivenga, "Characterization of ultrafast free-electron laser pulses using extreme-ultraviolet transient gratings," *J. Synchrotron Radiat.* **25**(1), 32–38 (2018).